Korea-Australia Rheology Journal, 30(1), 29-39 (February 2018) www.springer.com/13367
DOI: 10.1007/s13367-018-0004-z

A discrete element model for the influence of surfactants on sedimentation characteristics of magnetorheological fluids

Kwon Joong Son*
Department of Mechanical and Design Engineering, Hongik University, Sejong 30016, Republic of Korea
(Received August 16, 2017; final revision received November 1, 2017; accepted November 18, 2017)

Hindering particle agglomeration and re-dispersion processes, gravitational sedimentation of suspended particles in magnetorheological (MR) fluids causes inferior performance and controllability of MR fluids in response to a user-specified magnetic field. Thus, suspension stability is one of the principal factors to be considered in synthesizing MR fluids. However, only a few computational studies have been reported so far on the sedimentation characteristics of suspended particles under gravity. In this paper, the settling dynamics of paramagnetic particles suspended in MR fluids was investigated via discrete element method (DEM) simulations. This work focuses particularly on developing accurate fluid-particle and particle-particle interaction models which can account for the influence of stabilizing surfactants on the MR fluid sedimentation. Effect of the stabilizing surfactants on interparticle interactions was incorporated into the derivation of a reliable contact-impact model for DEM computation. Also, the influence of the stabilizing additives on fluid-particle interactions was considered by incorporating Stokes drag with shape and wall correction factors into DEM formulation. The results of simulations performed for model validation purposes showed a good agreement with the published sedimentation measurement data in terms of an initial sedimentation velocity and a final sedimentation ratio.

Keywords: sedimentation simulation, discrete element method, magnetorheological fluids, surfactants

1. Introduction

A magnetorheological (MR) fluid consists of three basic components: paramagnetic particles, carrier fluid, and additives (Phule, 2001). Chaining of the paramagnetic particles under an application of external magnetic field increases the yield stress of MR fluids (Jolly *et al*., 1999). This field-dependent rheological behavior makes MR fluids a suitable material for various smart damping applications such as semi-active vehicle suspension systems (McManus *et al*., 2002; Yao *et al*., 2002) and soft body armor systems (Kozlowska and Leonowicz, 2013; Son and Fahrenthold, 2012).

The dynamic behavior and performance of MR fluids are sensitive to the magnetomechanical properties of paramagnetic particles, the hydrodynamic properties of carrier fluids, and the physicochemical properties of additives. Hence, various kinds of MR fluids can be synthesized by varying the type and combination of the three constituents. Characterization and evaluation of the synthesized MR fluids have been performed using a rheometer equipped with permanent magnets or electromagnets to polarize and aggregate the suspended particles in a controllable way (Hato *et al*., 2011; Lim *et al*., 2005; Shah and Choi, 2015). The magnetic-field-induced structural transition of dispersed particles into aggregated chains on a micrometer scale has been observed using high-resolution microscopes such as a digital microscope (Dodbiba *et al*., 2008) and a scanning electron microscope (López-López *et al*., 2007; Zhang *et al*., 2012). On the other hand, the settling rate and sedimentation ratio due to gravity have been measured using an inductance meter (Chen and Chen, 2003) or simply by visual identification on a long-term basis (Fang *et al*., 2009; Hato *et al*., 2011; Lim *et al*., 2005; Shah and Choi, 2015). As mentioned above, most of the material properties of MR fluids can be experimentally obtained by currently available measurement techniques. Nevertheless, for material design purposes, computational characterization and prediction of MR fluid properties are more cost-effective and time-efficient in material design and manufacturing than purely experimental approaches.

Most of the previous computational investigations have focused on the simulation of magnetic-field-induced particle aggregation and the associated rheological behavior. Han *et al*. (2010) performed modeling and simulations for the particle chain formation under an external magnetic field and for the rheological response due to external shear loading. They employed a discrete element method (DEM) and Stokes hydrodynamics for chain formation simulations. The interparticle magnetostatic force and Stokes drag force were incorporated into the conventional discrete element method via an external body force to individual particles. On the other hand, a combined discrete element and lattice Boltzmann method was used in computing complex particle-fluid interactions under shear loading. Their magnetostatic and hydrodynamic interac-

*Corresponding author; E-mail: kjson@hongik.ac.kr

© 2018 The Korean Society of Rheology and Springer

tion models can compute the short-term responses associated with particle chaining and shearing on millisecond time scale. Climent *et al*. (2004) simulated the aggregation dynamics of paramagnetic particles in MR fluids by incorporating the magnetostatic attraction, hydrodynamic drag, and Brownian diffusion models into a two-way coupling method called the force coupling method (FCM). Their model specifically aimed at computing the transient particle aggregation dynamics of low-concentration MR fluids. The simulations results predicted the mean chain and magnetic dipole strengths length at varying particle concentrations. However, their mechanical contact-impact calculations were based on a too simplified repulsion model without consideration of the elastic-plastic deformation of impacted particles during the compression and restitution phases.

Numerical simulation can also calculate the packing density of paramagnetic particles (Dodbiba *et al*., 2008) and predict the particle sedimentation dynamics (Climent and Maxey, 2003; Sun and Xiao, 2016). Using DEM, Dodbiba *et al*. (2008) investigated the influence of particle sizes and mixing ratio on the packing density of a binary particle mixture. The packing density is closely related to the magnetic susceptibility of particle clusters and hence to interparticle cohesion forces that determine the performance of MR fluids. Climent and Maxey (2003) extended the force coupling method first introduced by Maxey *et al*. (1997) to model the sedimentation dynamics of quiescent suspensions at low Reynolds number conditions. Their numerical model can compute carrier fluid flows as well as suspended particle motions. The estimated mean sedimentation velocity using FCM showed a good agreement with the measured data. Sun and Xiao (2016) introduced the open-source and parallel DEM-CFD solver called SediFoam, which can carry out three-dimensional and two-phase flow simulations of particle-fluid suspensions. The inter-particle contact force is represented by a spring-dashpot model, and the fluid-particle interaction force was determined by the combined hydrodynamic effects such as drag, lift, buoyancy, and added mass. Such a DEM-CFD coupling approach is versatile in that it can solve complex particle-fluid interaction problems by preserving the benefits of each computational method. However, the DEM-CFD coupling approach suffers from high computational cost and a relatively complex parameter tuning procedure. If a solution accuracy is guaranteed, an uncoupled computational method is desirable for modeling dynamics of many-particle systems (Son and Fahrenthold, 2014) due to its computational efficiency. Therefore, an uncoupled but modified DEM approach was applied to this computational study of the micron-sized particle sedimentation in MR fluids.

In the above-stated studies by Han *et al*. (2010), Climent *et al*. (2004), Dodbiba *et al*. (2008), Climent and Maxey (2003), and Sun and Xiao (2016), the repulsion due to intermolecular forces in the presence of surfactants was not incorporated into the numerical simulations. However, stabilizing surfactants have been observed to play a significant role in interparticle repulsion and hence in suspension stability of MR fluids (Chen and Chen, 2003; Fang *et al*., 2005; Fang *et al*., 2009; Hato *et al*., 2011, Jang *et al*., 2005; Lim *et al*., 2005). The surfactants can surround iron particles and form a repulsive and low-stiffness coating layer. The increase in particle size due to surfactant coating enhances anti-settling hydrodynamics effects. Thus, this soft and dispersing surface layer may effectively reduce the particle sedimentation rate and consequently enhance the suspension stability of MR fluids (Fang *et al*., 2005). Incorporating the surfactant effects into DEM modeling is a key stage in this modeling and simulation research.

The particle forces that should be considered in DEM sedimentation analysis consist of the weight due to gravity, the contact forces due to collision with neighboring particles or wall boundaries, the hydrostatic buoyancy force, and the hydrodynamic drag force due to the viscosity of surrounding fluid. In addition to buoyancy and drag, an additional hydrodynamic effect, called the added mass effect (Falkovich, 2011), should be considered for a more accurate sedimentation simulation. The previous modeling studies on MR fluid sedimentation (Han *et al*., 2010; Climent *et al*., 2004) have utilized a Stokes drag model to calculate the drag force on a translating sphere under low Reynolds number conditions ($Re << 1$) without accounting for the added mass effect except in the cited reference by Climent and Maxey (2003). The Stokes model is based on the assumption that a single spherical particle is moving at a constant speed in an infinite fluid medium (Douglas *et al*., 2005). It neglects any contributions of neighboring particles or container walls to the hydrodynamic drag. In addition, the drag model employed in the previous studies on MR fluid sedimentation simulations takes into account neither the shape irregularities and surface roughness of paramagnetic particles nor the added mass effect.

Unlike previous computational work, this paper aims at developing a discrete element model suitable for simulating the transient settling of MR fluid particles by incorporating (1) the shape irregularities and surface roughness, (2) the added mass effect, and (3) the surfactant effects into the particle-particle contact model and the fluid-particle interaction model. A series of simulations were carried out to obtain the initial sedimentation velocity of MR fluid samples prepared with and without surfactants. The computational accuracy of the proposed DEM model is validated against the measured sedimentation data published in Fang *et al*. (2005).

The rest parts of this paper are organized as follows. The

next section derives the equation of motion of a micron-sized spherical particle settling down at a low Reynolds number in a viscous fluid. The equation of motion includes the particle-particle and particle-fluid interaction terms that can also account for the surfactant effects. The section that follows describes the procedure and results of simulations that were conducted to evaluate the validity of the derived discrete element model. Lastly, the final section draws general conclusions about this computational study.

2. Modeling

Sedimentation hinders the paramagnetic particles in MR fluids from promptly forming columnar agglomerates. Interruption of the structural transition of particles may significantly degrade the shear thickening capability of MR fluids under an external magnetic field. Anti-sedimentation equipment such as shakers and mixers are often used to avoid sedimentation problems in some other particle suspensions like concrete. However, due to simplicity and sustainability, an intrinsic anti-sedimentation capability of MR fluids is preferred to the use of additional anti-sedimentation equipment. One of the most widely used anti-sedimentation techniques is the addition of stabilizing surfactants to MR fluids (Fang *et al*., 2005; Fang *et al*., 2009; Hato *et al*., 2011; Jang *et al*., 2005; Lim *et al*., 2005; Wu *et al*., 2006). Anti-settling surfactants surrounding and coating the suspended particles in MR fluids can continuously prevent the particles from being deposited. From a modeling point of view, first of all, the surfactants increase the particle size that affects the resultant hydrodynamic force as well as the particle inertia. Secondly, the surfactants much more compliant than the particle material dramatically reduce the contact stiffness. Lastly, the micron- or submicron-sized surfactants left dissolved in the solution increase the fluid viscosity. In this section, a discrete element model for suspended particles in MR fluids is formulated in consideration of the influence of surfactants on particle-particle and fluid-particle interactions.

2.1. Equation of motion

The equation of motion for a paramagnetic particle i in a magnetorheological fluid is

$$(m_p^{(i)}+m_a^{(i)})\frac{d\overline{\mathbf{u}}^{(i)}}{dt} = \overline{\mathbf{F}}_M^{(i)} + \overline{\mathbf{F}}_G^{(i)} + \Sigma_{\substack{j=1\\ j\neq i}}^{n}\overline{\mathbf{F}}_C^{(i,j)}+\overline{\mathbf{F}}_B^{(i)}+\overline{\mathbf{F}}_D^{(i)}+\overline{\mathbf{F}}_W^{(i)} \quad (1)$$

where $m_p^{(i)}$ is the particle mass $m_a^{(i)}$ is the added mass, $\overline{\mathbf{u}}^{(i)}$ is the particle center-of-mass velocity vector, $\overline{\mathbf{F}}_M^{(i)}$ is the magnetic force, $\overline{\mathbf{F}}_G^{(i)}$ is the weight due to gravity, $\overline{\mathbf{F}}_C^{(i,j)}$ is the contact force exerted by neighboring particle j, $\overline{\mathbf{F}}_B^{(i)}$ is the buoyancy force, $\overline{\mathbf{F}}_D^{(i)}$ is the drag force due to fluid viscosity, and $\overline{\mathbf{F}}_W^{(i)}$ the resultant force of other weak forces such as Van der Waals forces and Brownian forces. In this study, the magnetic force $\overline{\mathbf{F}}_M^{(i)}$ and the weak force $\overline{\mathbf{F}}_W^{(i)}$ are neglected. Modeling magnetic interactions under an application of external magnetic field is beyond the interest of this study focusing on the settling dynamics of non-magnetized particles, but a comprehensive review on magnetic force modeling can be found in Han *et al*. (2010). In addition, the weak molecular forces and thermal fluctuations are negligible for micron-sized iron particles at room temperature (Ly *et at*., 1999). Hence, the equation of motion used in this simulation study can be reduced to the form as below.

$$(m_p^{(i)}+m_a^{(i)})\frac{d\overline{\mathbf{u}}^{(i)}}{dt} = \overline{\mathbf{F}}_G^{(i)} + \Sigma_{\substack{j=1\\ j\neq i}}^{n}\overline{\mathbf{F}}_C^{(i,j)}+\overline{\mathbf{F}}_B^{(i)}+\overline{\mathbf{F}}_D^{(i)} \quad (2)$$

with

$$\overline{\mathbf{F}}_G^{(i)} = \rho_p^{(i)} V^{(i)}\overline{\mathbf{g}} \quad (3)$$

where ρ_p is the particle mass density, V is the particle volume, and $\overline{\mathbf{g}}$ is the gravitational acceleration vector. It should be noted that the density for the surfactant-coated particle is an apparent density.

2.2. Particle-particle interactions

The contact force term $\overline{\mathbf{F}}_C^{(i,j)}$ in Eq. (2) can be further decomposed into the normal component $\overline{\mathbf{F}}_{C,n}^{(i,j)}$ and the tangential component $\overline{\mathbf{F}}_{C,t}^{(i,j)}$ in an additive manner such that $\overline{\mathbf{F}}_C^{(i,j)} = \overline{\mathbf{F}}_{C,n}^{(i,j)} + \overline{\mathbf{F}}_{C,t}^{(i,j)}$. Among various contact models for discrete element analysis (Kruggel-Emden *et al*., 2007; Kruggel-Emden *et al*., 2008), this study uses the modified Hertz model and the Mindlin model to calculate the viscoelastic normal and tangential contact forces, respectively. These contact models are beneficial in the sense that their model parameters can be derived from the elastic materials properties such as Young's modulus and Possion's ratio.

The normal viscoelastic contact force extended from the classical Hertzian elastic contact model (Pöschel and Schwager, 2005) can be expressed as a function of the overlap distance $\delta^{(i,j)}$ depicted in Fig. 1 and its time derivative $\dot{\delta}^{(i,j)}$ by

$$\overline{\mathbf{F}}_{C,n}^{(i,j)} = \frac{4}{3}E_{\text{eff}}^{(i,j)}\sqrt{R_{\text{eff}}^{(i,j)}\delta^{(i,j)}}(\delta^{(i,j)} - A^{(i,j)}\dot{\delta}^{(i,j)})H(\delta^{(i,j)})\hat{\mathbf{n}}^{(i,j)} \quad (4)$$

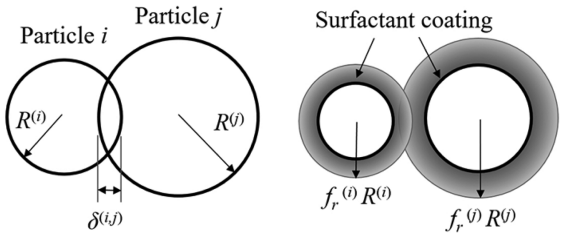

Fig. 1. (Color online) Illustration of the contact overlap $\delta^{(i,j)}$ between two particles with radii of $R^{(i)}$ and $R^{(j)}$ (left) and that between surfactant-coated particles with radius magnification factors $f_r^{(i)}$ and $f_r^{(j)}$ (right).

where $E_{\text{eff}}^{(i,j)}$ is the effective modulus of elasticity, $R_{\text{eff}}^{(i,j)}$ is the effective radius, H is the Heaviside step function, $A^{(i,j)}$ is the dissipative coefficient that is related to material damping and thus the coefficient of restitution as discussed in details in Tsuji *et al*. (1992), and $\hat{\mathbf{n}}^{(i,j)}$ is a unit directional vector along the center-to-center direction from particle j to particle i. The effective modulus of two colliding elastic spheres i and j is written as

$$\frac{1}{E_{\text{eff}}^{(i,j)}} = \frac{1-\nu^{(i)^2}}{E^{(i)}} + \frac{1-\nu^{(i)^2}}{E^{(j)}} \tag{5}$$

where E and ν denote the elastic modulus and the Poisson's ratio, respectively, for each particle. The effective radius of two colliding spheres of radius $R^{(i)}$ and $R^{(j)}$ is given by

$$\frac{1}{R_{\text{eff}}^{(i,j)}} = \frac{1}{R^{(i)}} + \frac{1}{R^{(j)}} \tag{6}$$

The tangential viscoelastic contact force from the work of Tsuji *et al*. (1992) can be rewritten in a similar form to Eq. (4) as

$$\overline{\mathbf{F}}_{C,t}^{(i,j)} = 8G_{\text{eff}}^{(i,j)}\sqrt{R_{\text{eff}}^{(i,j)}\delta^{(i,j)}}(\delta_t^{(i,j)} - B^{(i,j)}\dot{\delta}_t^{(i,j)})H(\delta^{(i,j)})\hat{\mathbf{t}}^{(i,j)} \tag{7}$$

where δ_t is the tangential overlap, $\dot{\delta}_t$ is the tangential overlap velocity, $B^{(i,j)}$ the dissipative coefficient, $\hat{\mathbf{t}}^{(i,j)}$ is a unit directional vector perpendicular to $\hat{\mathbf{n}}^{(i,j)}$ in Eq. (4), and $G_{\text{eff}}^{(i,j)}$ is the effective modulus of rigidity given by

$$\frac{1}{G_{\text{eff}}^{(i,j)}} = \frac{2-\nu^{(i)}}{G^{(i)}} + \frac{2-\nu^{(j)}}{G^{(j)}} \tag{8}$$

It should be noted that the magnitude of $\overline{\mathbf{F}}_{C,t}^{(i,j)}$ computed from the spring-dashpot representation must be limited by the kinematic Coulomb friction force.

2.3. Particle-fluid interactions

MR fluids are a fluid-particle mixture whose dynamics is determined by the coupled motion of immersed particles and a base fluid. The flow simulation of the base fluid using computational fluid dynamics is not the main concern of this sedimentation simulation study. A simple but reliable method is to incorporate hydrodynamic interactions such as buoyancy, drag, and added mass into the calculation of particle motion with no CFD analysis.

The buoyancy force on an immersed particle i is

$$\overline{\mathbf{F}}_G^{(i)} = \rho_f V^{(i)}\overline{\mathbf{g}} \tag{9}$$

where ρ_f is the fluid density. A hydrodynamic drag force on a spherical particle i at a low Reynolds number can be calculated using the following Stokes' formula (Douglas *et al*., 2005).

$$\overline{\mathbf{F}}_D^{(i)} = -6\pi\mu R^{(i)}\overline{\mathbf{u}}^{(i)} \tag{10}$$

where μ is the fluid viscosity. The added mass for particle i is given by

$$m_a^{(i)} = \frac{1}{2}\rho_f V^{(i)} \tag{11}$$

when the fluid is stationary and incompressible. The added mass is a virtual inertia of a fluid volume which should be removed and accelerated before being occupied by a solid particle in motion (Falkovich, 2011).

The closed-form solution of Eq. (2) may help better understand the influence of hydrodynamic forces given in Eqs. (9)-(11) on the sedimentation of particles. The difficulty in obtaining an analytical solution arises from the fact that the contact forces expressed in Eqs. (4) and (7) are nonlinear. An analytical solution exists in an ideal case where there are no particle-to-particle interactions, *i.e.*, the case where only a single spherical particle is settling due to gravity in a quiescent fluid medium. Being modified from Eqs. (2), (3), (9), (10), and (11), the one-dimensional form of the equation of motion for a spherical particle slowly moving in the direction parallel to gravity can be written as

$$(m_p + m_a)\dot{u} = F_G - F_B - F_D \tag{12}$$

where u and $\dot{u}$ are the speed and acceleration of the particle, respectively, the force due to gravity is $F_G = \frac{4\pi}{3}R^3\rho_p g$, the buoyance force is $F_B = \frac{4\pi}{3}R^3\rho_f g$, and the Stoke's drag force is $F_D = 6\pi\mu R u$.

Solving the differential equation of Eq. (12) for the zero-velocity initial condition yields the following closed-form solution for the sphere velocity.

$$v(t) = \frac{\beta}{\alpha}(1 - e^{-\alpha t}) \tag{13}$$

where $\alpha = \frac{9}{2}\frac{\mu}{\rho_p R^2}$ and $\beta = \left(1 - \frac{\rho_f}{\rho_p}\right)g$. Especially, the leading coefficient β/α in Eq. (13) is the steady-state settling velocity of the sphere immersed in a viscous fluid. With the properties of Table 1, the steady-state velocity of a carbonyl iron particle of 4-μm diameter immersed in a silicon oil is 491.2 mm/day. The Reynolds number associated

Table 1. Physical and geometric properties of the MR fluid constituents.

Property	Unit	Carbonyl iron	Silicone oil	Hydrated guar gum
Mean diameter	μm	4	–	–
Density	kg/m^3	7470	950	800
Viscosity	Pa·s	–	0.01	–
Elastic modulus	GPa	211	–	3120
Poisson's ratio	–	0.31	–	0.25

with this calculation result of settling velocity is Re = 2.167×10^{-6}, which satisfies the Stokes flow condition Re << 1. However, the analytical solution significantly overestimates the sedimentation speed more than 60 times greater than the measured settling rate of 8 mm/day from Fang *et al*. 2005. Such an overestimation is mainly caused by the underestimation of the Stokes drag force in Eq. (10). Such a computational error due to the underestimated hydrodynamic drag is not apparent in the simulation of a short-term particle aggregation which takes place in a few milliseconds upon application of magnetic field to MR fluids. However, in the simulation of MR fluid sedimentation that occurs over a long-term period (several days or even several months), a computational error due to the inaccurate estimation of the Stokes drag is quite large. Therefore, for the use in this sedimentation simulation, the Stokes drag model in form of Eq. (10) should be modified by appropriate correction factors that can account for real situations where there are many particles surface irregularities of some degree.

One of the correction factors to the Stokes drag is a wall correction factor. It is defined by the ratio of the drag force in a finite fluid medium bounded by wall boundaries or neighboring particles to that in an infinite medium, *i.e.*, the Stokes drag force in Eq. (10). Haberman and Sayre (1958) modeled a wall correction factor for a rigid sphere settling in a stationary fluid inside a cylindrical tube. Their correction factor was expressed in the form of the rational polynomial about the diameter ratio which denotes the ratio of the sphere dimeter to the tube diameter. On the other hand, this study uses the following form of the correction factor that was fitted to the data published in Haberman and Sayre (1958) as shown in Fig. 2.

$$f_w = \mathrm{MIN}(f_w^{\max}, 389.1530\lambda^{7.5593}+1) \tag{14}$$

where f_w is the wall correction factor, MIN is the minimum function that returns the minimum value of the arguments, $f_w^{\max}$ the upper limit of f_w, and λ the diameter ratio that quantifies the closeness of a particle to a solid wall. In this study, a modified diameter ratio in the following form is proposed to approximate the closeness of a particle to the neighboring solid particles in addition to the container wall.

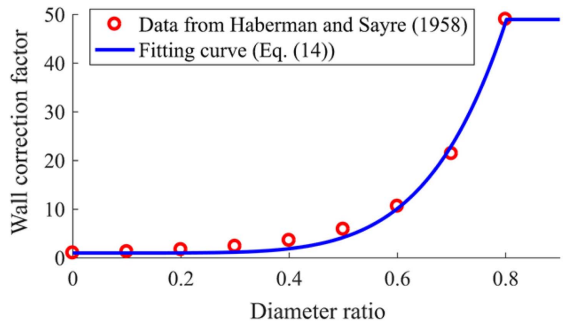

Fig. 2. (Color online) Wall correction factor versus diameter ratio data published in Haberman and Sayre (1958) and the regression curve fit in Eq. (14).

$$\lambda = \left(\sqrt[3]{\frac{4\pi}{3\phi_p}} - 1\right)^{-1} \tag{15}$$

where ϕ_p is the volume fraction of the particles dispersed in an MR fluid. The upper limit of the wall correction factor $f_w^{\max}$ is set to 48.985 which is the value approximated by Haberman and Sayre (1958) when $\lambda = 0.8$.

The other correction factor to the Stokes drag considered in this study is a shape correction factor. It reflects the influence of shape irregularity and surface smoothness of the particle moving in a viscous fluid on a hydrodynamic drag force. One of the widely used regression models proposed by Loth (2008) is given by

$$f_s = A_{\mathrm{mmm}}^{0.09} \tag{16}$$

where f_s is the shape correction factor, and A_{mmm} is the dimensionless max-med-min area defined by

$$A_{\mathrm{mmm}} = \frac{d_{\max} d_{\mathrm{med}}}{d_{\min}^2} \tag{17}$$

where $d_{\max}$ the maximum dimension, d_{med} the medium dimension, and $d_{\min}$ is the minimum dimension of an irregular, non-spherical particle.

Incorporating the two correction factors f_w and f_s into Eq. (10) yields the following modified Stokes drag model for particle *i*.

$$\overline{\mathbf{F}}_D^{(i)} = -6\pi f_w f_s \mu R^{(i)} \overline{\mathbf{u}}^{(i)}. \tag{18}$$

In Eq. (18), the drag force proportionally increases with the total Stokesian drag correction factor $f_w f_s$. Consequently, the steady-state settling velocity β/α in Eq. (13) is inversely proportional to the product $f_w f_s$. It should be noted an accurate application of drag corrections is very important to calculate the particle settling velocity.

2.4. Effects of stabilizing additives

An organic surfactant that can surround and coat paramagnetic particles dispersed in MR fluids is used to enhance the suspension stability. The surfactants have been observed to thicken suspension fluid, increase the particle size, and soften the contact stiffness.

Firstly, the micron- or submicron-sized surfactants left dissolved in the solution without being adsorbed onto metallic particles may impede the shear motion of the base fluid and hence increase its viscosity (Casas *et al*., 2000). The increase in fluid viscosity can be quantified with a viscosity magnification factor f_v that is defined by the ratio of the viscosity of the fluid containing surfactants to the viscosity of the original base fluid. It can be experimentally measured by standard rheometry techniques (Fang *et al*., 2009; Hato *et al*., 2011).

Secondly, the increase in particle size due to the coating can be modeled with a radius magnification factor f_r that is defined by the ratio of the surfactant-coated particle radius to the intact particle radius as illustrated in Fig. 1. If a particle i with the radius of $R^{(i)}$ and the density of ρ_p is coated by surfactants with the density of ρ_c, the equation of motion in Eq. (2) for the coated particle can be rewritten as

$$(m_{cp}^{(i)}+m_{cp,a}^{(i)})\frac{d\overline{\mathbf{u}}^{(i)}}{dt} = \overline{\mathbf{F}}_G^{(i)} + \Sigma_{\substack{j=1 \\ j\neq i}}^{n}\overline{\mathbf{F}}_C^{(i,j)}+\overline{\mathbf{F}}_B^{(i)}+\overline{\mathbf{F}}_D^{(i)} \tag{19}$$

with

$$m_{cp}^{(i)} = [\rho_p+\rho_c(f_r^3-1)]V^{(i)}, \tag{20}$$

$$m_{cp,a}^{(i)} = \frac{1}{2}\rho_f f_r^3 V^{(i)}, \tag{21}$$

$$\overline{\mathbf{F}}_G^{(i)} = [\rho_p+\rho_c(f_r^3-1)]V^{(i)}\overline{\mathbf{g}}, \tag{22}$$

$$\overline{\mathbf{F}}_B^{(i)} = -\rho_f f_r^3 V^{(i)}\overline{\mathbf{g}}, \tag{23}$$

$$\overline{\mathbf{F}}_D^{(i)} = -6\pi f_w f_s f_v f_r \mu R^{(i)}\overline{\mathbf{u}}^{(i)} \tag{24}$$

where $m_{cp}^{(i)}$ is the mass of coated particle i and $m_{cp,a}^{(i)}$ is the corresponding added mass. The modification of contact model is discussed in the next paragraph.

Thirdly and lastly, the effect of the compliant coating on the interparticle contact forces can be considered by an appropriate stiffness model. Since the normal and shear stiffness values associated with the nonlinear contact models in Eqs. (4) and (7) are non-constant, the contact stiffness is defined as a tangential stiffness in the following differential form.

$$dF = K(\delta)d\delta \tag{25}$$

Paramagnetic particles coated with surfactants in MR fluids have a high-stiffness core and a low-stiffness coating layer as shown in Fig. 1. Such inhomogeneous particles have a piecewise smooth but discontinuous tangent stiffness as schematically illustrated in Fig. 3 where K_{ss}, K_{sh}, and K_{hh} denote the tangent stiffness between soft surfactants, between the surfactant and hard particle, and between hard metallic particles, respectively. If the penetration depth is extremely high, the tangential stiffness is contributed by all of the three stiffness values. However, if the overlap distance is much smaller than the thickness of coating layer, only K_{ss} is effective in the normal interaction of colliding particles. This small δ case occurs when the momentum of colliding particles is not high enough to result in the overlap between the surfactant layer and the iron particle core. The settling particles in a quiescent MR fluid move at very low velocity due to the significant viscous effects compared to the inertia effect. The momentum associated with the impact between settling particles is low enough to satisfy the above-mentioned small δ condition. Therefore, in the sedimentation simulations of MR fluids, the contact model parameters for the coated particles are computed based on the physical properties of a soft coating material.

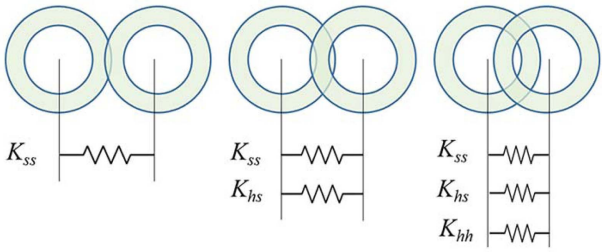

Fig. 3. (Color online) Schematic illustration of contact stiffness ($K_{ss} < K_{hs} << K_{hh}$) based on the degree of penetration depth between the particles with a soft coating layer and a hard inner core: soft-to-soft contact (left), soft-to-hard contact (middle), and hard-to-hard contact (right).

2.5. Computational time step

A proper choice of a computational time step for explicit integration in DEM simulations is important for the sake of both computational efficiency and accuracy. A too large time step may cause an extremely high contact force and a sudden unphysical scattering of particles. On the other hand, a too small time step leads to an excessively high computational time. At least, it should be chosen as a value smaller than the critical Rayleigh time step (Ren *et al*., 2012), which is given by

$$t_c = \frac{\pi R}{0.1631\nu+0.8766}\sqrt{\frac{\rho_p}{G}} \tag{26}$$

where G is the modulus of rigidity. This Rayleigh time step is related to the particle dimension (*i.e.*, R), the particle inertia (*i.e.*, ρ_p), and the particle elastic properties (*i.e.*, ν and G).

Especially, in this simulation study, the transient kinematics due to hydrodynamic forces on a settling particle should also be considered in the choice of the computational time step. The closed-form solution similar to Eq. (13) is useful to determine the time interval within which the transient particle kinematics can be computationally well approximated. Solving the differential equation of Eq. (19) with Eqs. (20) - (24) for the zero-velocity initial condition gives the following closed-form solution for an one-dimensional sedimentation velocity $v_c(t)$ of a coated particle

$$v_c(t) = \frac{\beta_c}{\alpha_c}(1-e^{-\alpha_c t}) \tag{27}$$

where $\alpha_c = \frac{9f_w f_s f_v \mu}{(2\rho_c+\rho_f)f_r^2 R^2}$ and $\beta_c = \left[\frac{2\rho_c-2\rho_f}{2\rho_c+\rho_f}\right]g$. From Eq.

(27), the rise time t_r is defined as the time required for the particle velocity to rise from 0 to 99% of its steady state value β_c/α_c, and can be expressed as

$$t_r = \frac{1}{\alpha_c}\ln\left[1-0.99\frac{\alpha_c}{\beta}\right]^{-1}. \quad (28)$$

A computational time step should be smaller than t_c and t_r to avoid solution instability due to the overestimation of contact force and to capture the hydrodynamic effects on the sedimentation velocity, respectively. In this study, computational time step Δt is chosen as

$$\Delta t \le \frac{\mathrm{MIN}(t_c, t_r)}{h_t} \quad (29)$$

where h_t is the time refinement factor.

3. Sedimentation Simulation Results and Discussions

A discrete element model including hydrodynamic and contact interactions has been derived in the previous section to simulate the sedimentation of MR fluids with and without organic surfactants. For computational analysis, the derived discrete element model, *i.e.*, Eqs. (19) - (24) and the computational time step discussed in this section, *i.e.*, Eq. (29) were integrated into the commercial code EDEM developed by DEM Solutions Inc. by using an application programming interface (API) through which user-defined particle kinematics and kinetics can be implemented. For the purpose of model validation, three cases of sedimentation simulations have been performed: (Case 1) sedimentation of surfactant-free particles without any Stokes drag corrections; (Case 2) sedimentation of surfactant-free particles with Stokes drag corrections; and (Case 3) sedimentation of surfactant-coated particles with considerations of the corrections for both hydrodynamic and contact interactions.

The two simulation outputs interested in this study are (1) the initial sedimentation velocity and (2) the final sedimentation ratio (Shah and Choi, 2015). The sedimentation velocity is defined by the rate at which a boundary between the sediment and the supernatant descends. The final sedimentation ratio is the ratio of the height of completely settled particles to that of initially well-dispersed particles. Those two output values are compared with experimental data for model validation purposes. The two sedimentation properties obtained from the validated computational model may be used to draw an asymptotic sedimentation ratio versus time curve that can characterize the sedimentation dynamics of MR fluids. Figure 4 shows a general sedimentation ratio versus time curve that can be approximated by two piecewise and continuous lines that represent the initial sedimentation rate and the final sedimentation ratio. It should be noted that the full transient

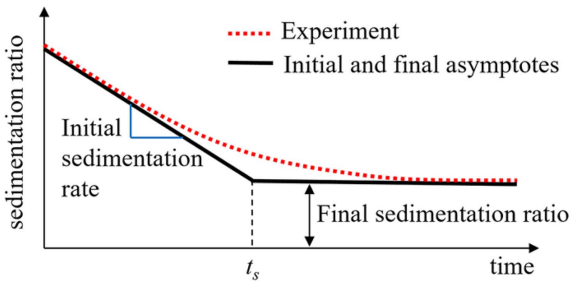

Fig. 4. (Color online) Typical sedimentation ratio versus time curve (dotted line) and piecewise linear initial and final asymptotes (solid lines).

profile of the gravitational sedimentation of MR fluids could be also obtained using the discrete element model derived in the previous section. However, this simulation work specifically targeted at computing the initial and final sedimentation characteristics due to an extremely long computational time required for the entire initial to final sedimentation behavior.

3.1. Sedimentation simulation without Stokes drag corrections

The first simulation, designated as Case 1, was carried out based on the equation of motion in Eq. (2) by setting $m_a^{(i)}=0$ and using the uncorrected Stokes drag model in Eq. (10). This simulation condition was considered to check if the particle and hydrodynamic models used in previous computational studies on a short-term phase change in MR fluids subject to an external magnetic field (Climent *et al*., 2004; Han *et al*., 2010) are also applicable to the simulation of the long-term sedimentation phenomenon.

The material composition for Case 1 simulation is identical to that of the MR fluid denoted as sample A in Fang *et al*. (2005). It consists of 80 wt.% carbonyl iron particles

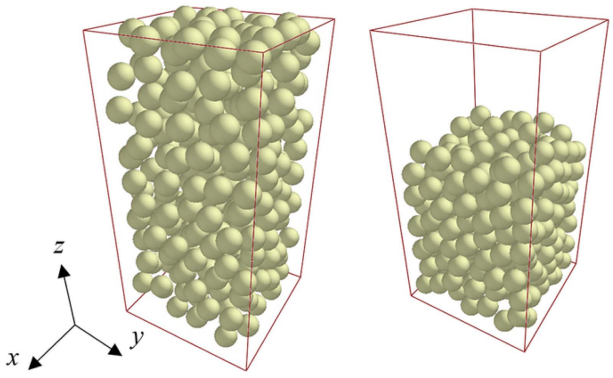

Fig. 5. (Color online) Uniform 314 spheres of 4 μm diameter randomly dispersed in a 25×25×50 μm^3 cuboidal volume which represents an MR fluid sample consisting of 80 wt.% carbonyl iron particles and 20 wt.% carrier oil (left), and fully settled particles (right).

Table 2. Input parameters and calculation results of three simulation cases.

Property	Unit	Case 1	Case 2	Case 3
Surfactant weight composition	%	0.0	0.0	1.6
Shape correction factor	–	1.00	1.10	1.10
Wall correction factor	–	1.00	48.49	48.99
Radius magnification factor	–	1.00	1.00	1.10
Viscosity magnification factor	–	1.00	1.00	1.68
Computation time step	nanosecond	100.0	0.1	1.0
Initial settling velocity (Fang *et al*., 2005)	mm/day	8.0	8.0	3.6
Initial settling velocity (Simulation)	mm/day	491.2	9.2	4.0
Reynolds number	–	2.16×10^{-6}	2.41×10^{-8}	6.82×10^{-9}
Final sedimentation ratio (Fang *et al*., 2005)	%	78.0%	78.0%	90.0%
Final sedimentation ratio (Simulation)	%	69.3%	69.3%	86.4%

and 20 wt.% synthetic silicone oil, properties of both of which are listed in Table 1. Because sample A contains no stabilizing additives, the suspended particles are not coated. The measured initial sedimentation velocity of sample A was 8 mm/day, and the final sedimentation ratio was 78%. In Case 1 simulation, a 25×25×50 μm^3 cuboidal volume was chosen as a computational domain. The cuboid should contain 314 uniform carbonyl iron particles of 4 μm diameter to have the same size and weight fraction of carbonyl iron as sample A. Figure 5 shows the initial configuration of the randomly distributed particles and the final settled configuration. The final configuration was obtained from a settling simulation excluding hydrodynamic interactions for computational efficiency after a steady initial sedimentation velocity is determined. The simulation input parameters and the numerical results are listed in Table 2.

The initial sedimentation velocity and final sedimentation ratio computed by DEM were 491.2 mm/day and 69.3%, respectively. It should be noted that the initial sedimentation velocity was overestimated more than 60 times greater than the measured settling velocity in Fang *et al*. (2005). It is evident that the uncorrected Stokes drag model is not applicable in this study due to poor accuracy. This inaccuracy issue would be insignificant in the MR fluid magnetization simulations (Climent *et al*., 2004; Han *et al*., 2010) not only because the characteristic time associated with the field-induced phase transition of MR fluids is very short (*e.g.*, on the order of milliseconds) compared to that of MR fluid sedimentation (*e.g.*, on the order of days or even months), but because a hydrodynamic drag on magnetized particles is not a dominant force compared to a magnetic force in a chaining situation unlike that on unmagnetized particles in a settling state. The necessity and effect of Stokes drag corrections are studied in Case 2 simulation that follows.

3.2. Sedimentation simulation with Stokes drag corrections

The second simulation, designated as Case 2, incorporates Stokes drag corrections in Eq. (18) and added mass in Eq. (11) into a sedimentation analysis. These simulation conditions in Case 2 were chosen to better emulate the sedimentation characteristics of MR fluids than those in Case 1. The MR fluid composition for Case 2 simulation is the same as that for Case 1 simulation, and hence the initial and final configurations of the modeled particles are identical to those for Case 1 as shown in Fig. 5.

The computed initial sedimentation velocity was 9.2 mm/day, that is 15% greater than the experimental value of 8 mm/day as shown in the bar chart in Fig. 6. It verifies that the Stokes drag correction and the virtual mass addition can significantly improve the computational accuracy in the prediction of a settling rate. The calculated final sedimentation ratio was 69.3%, which is 11.2% less than the measured value of 78% as shown in the bar chart in Fig. 7. The overestimation of the settling rate and the

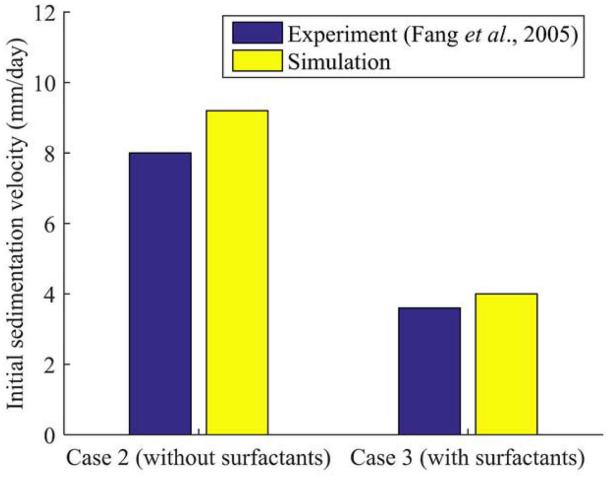

Fig. 6. (Color online) Comparison of the simulation results on the initial sedimentation velocity for the surfactant-free MR fluid (Case 2) and the surfactant-added MR fluid (Case 3) with the experimental results from Fang *et al*. (2005).

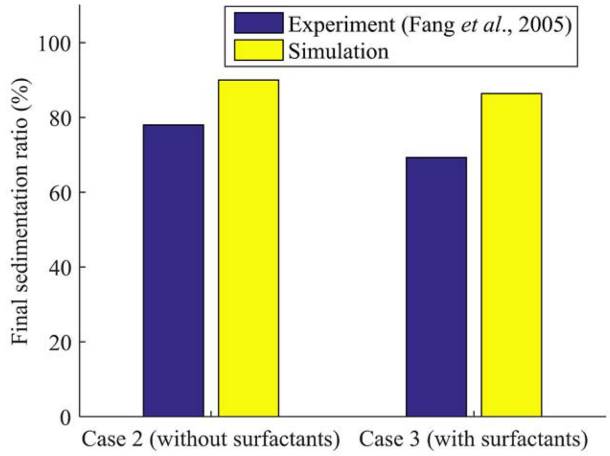

Fig. 7. (Color online) Comparison of the simulation results on the final sedimentation ratio for the surfactant-free MR fluid (Case 2) and the surfactant-added MR fluid (Case 3) with the experimental results from Fang *et al*. (2005).

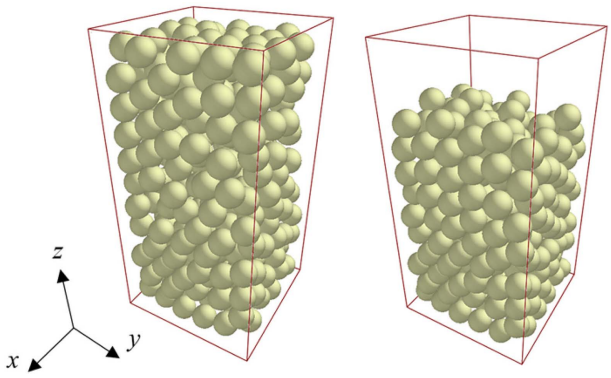

Fig. 8. (Color online) Uniform 292 spheres of 4.4 μm diameter randomly dispersed in a 25×25×50 μm^3 cuboidal volume which represents an MR fluid sample consisting of 78.4 wt.% carbonyl iron particles, 20 wt.% carrier oil, and 1.6 wt.% guar gum surfactants (left), and completely settled particles (right).

underestimation of final sedimentation ratio would be due to the neglection of the shape and size irregularities of the particles in this simulation. The particles smaller than the mean particle size would settle at a velocity lower than the computed value. The shape irregularities would increase the particle packing ratio, and hence increase the final sedimentation ratio. However, the influences of shape irregularity and size non-uniformity are out of the scope of this modeling and simulation work.

3.3. Sedimentation simulation of surfactant-coated particles

The third simulation, designated as Case 3, was performed to validate the DEM model developed for the case where surfactant additives are applied to MR fluids. The additives change the base fluid viscosity, particle size, and contact stiffness as previously discussed in Section 2.4. Such phenomenological changes in the MR fluid properties were incorporated into the sedimentation simulation through the DEM model that is comprised of the equation of motion in Eq. (19), the mass inertias in Eqs. (20) and (21), the contact forces in Eqs. (4) and (7) with the tangential contact stiffness in Eq. (25), and other body forces in Eqs. (22) and (23).

The material composition was chosen to mimic that of the MR fluid referred to as sample B in Fang *et al*. (2005). It consists of 78.4 wt.% carbonyl iron particles, 20.0 wt.% silicone oil, and 1.6 wt.% guar gum surfactants. The material properties of three constituents are listed in Table 1. The experimental initial sedimentation velocity and the final sedimentation ratio of sample B were 3.6 mm/day and 90%, respectively.

The same 25×25×50 μm^3 cuboidal volume as in the proceeding simulations was selected as a computational domain for Case 3 simulation. The domain must consist of 292 spheres to represent the weight fraction of carbonyl iron particles in sample B. Figure 8 depicts the initial and final configurations of sample B particles. The viscosity magnification factor f_v was set to 1.68 in this simulation based on the rheological data from Fang *et al*. (2005), where the viscosity of sample B was observed to be 1.68 times greater than that of sample A at the shear strain rate of 50 s^{-1}. A 10% increase in particle diameter, *i.e.*, a radius magnification factor f_r of 1.1, was estimated from the scanning electron microscopy image of a carbonyl iron particle completely coated by guar gum in Wu *et al*. (2006). The computation results, as well as the simulation other input parameters, are given in Table 2.

The initial sedimentation velocity and the final sedimentation ratio obtained from Case 3 simulation were 4.0 mm/day and 86.4%, respectively. Compared to the experimental data, as shown in Figs. 6 and 7, the initial sedimentation velocity was 11.1% overestimated, and the final sedimentation ratio was 4.0% overestimated. Despite some computational error within maximum 15%, the calculated values using the proposed discrete element model are in satisfactory agreement with the experimental data. Most of all, to the author's knowledge, the proposed model is the first one that can numerically compute the sedimentation characteristics of MR fluids by accounting for the influence of stabilizing surfactants on the carrier fluid viscosity, the particle volume dilation, and the inter-particle contact stiffness.

4. Conclusions

This research aims at developing a reliable computational model to predict the sedimentation characteristics of MR fluids containing stabilizing surfactants. A discrete element approach was used to model particle-to-particle

and particle-to-fluid interactions. The limitation of uncorrected Stokes drag model in the sedimentation simulation of MR fluids with the high volume fraction of paramagnetic particles was demonstrated by the discrete element simulation giving a large computational error. The numerical accuracy was significantly improved by the correction of the Stokes drag model and the inclusion of added mass effect into the equation of motion. This paper also presents the extended discrete element model that can predict the initial settling velocity of the suspended particles in MR fluids with added surfactants by introducting the four simulation parameters, *i.e.*, the wall correction factor, the shape correction factor, the radius magnification factor, and the viscosity magnification factor. The surfactants surrounding and coating the MR fluid particles may increase the particle dimensions, reduce the contact stiffness, and augment the carrier fluid viscosity. All of these possible phenomenological changes were incorporated into the discrete element formulation. The performed settling simulation well represented the influences of the stabilizing surfactants, and the simulation results matched the measured initial sedimentation velocity and final sedimentation ratio with acceptable accuracy. The proposed model is the first one which can compute the sedimentation characteristics of MR fluids containing surfactant additives, and thus can contribute to the material design and production of a stable MR fluid. Future work may include the further improvement of computational accuracy in the sedimentation analysis by taking the effects of non-uniform size distribution and non-spherical particle shapes into account.

Acknowledgements

This work was supported by 2016 Hongik University Research Fund and was also supported in part by Basic Science Research Program through the National Research Foundation of Korea (NRF) funded by the Ministry of Education (Grant number: 2016R1D1A1B03936214).

References

Casas, J.A., A.F. Mohedano, and F. García-Ochoa, 2000, Viscosity of guar gum and xanthan/guar gum mixture solutions, *J. Sci. Food Agric.* **80**, 1722-1727.

Chen, L.S. and D.Y. Chen, 2003, Permalloy inductor based instrument that measures the sedimentation constant of magnetorheological fluids, *Rev. Sci. Instrum.* **74**, 3566-3568.

Climent, E. and M.R. Maxey, 2003, Numerical simulations of random suspensions at finite Reynolds numbers, *Int. J. Multiph. Flow* **29**, 579-601.

Climent, E., M.R. Maxey, and G.E. Karniadakis, 2004, Dynamics of self-assembled chaining in magnetorheological fluids, *Langmuir* **20**, 507-513.

Dodbiba, G., H.S. Park, K. Okaya, and T. Fujita, 2008, Investigating magnetorheological properties of a mixture of two types of carbonyl iron powders suspended in an ionic liquid, *J. Magn. Magn. Mater.* **320**, 1322-1327.

Douglas, J.F., J.M. Gasoriek, J.A. Swaffield, and L.B. Jack, 2005, *Fluid Mechanics*, 5th ed., Pearson, London.

Falkovich, G., 2011, *Fluid Mechanics: A Short Course for Physicists*, Cambridge University Press, New York.

Fang, C., B.Y. Zhao, L.S. Chen, Q. Wu, N. Liu, and K.A. Hu, 2005, The effect of the green additive guar gum on the properties of magnetorheological fluid, *Smart Mater. Struct.* **14**, N1-N5.

Fang, F.F., H.J. Choi, and M.S. Jhon, 2009, Magnetorheology of soft magnetic carbonyl iron suspension with single-walled carbon nanotube additive and its yield stress scaling function, *Colloids Surf., A-Physicochem. Eng. Asp.* **351**, 46-51.

Haberman, W.L. and R.M. Sayre, 1958, Motion of rigid and fluid spheres in stationary and moving liquids inside cylindrical tubes, *Hydromechanics Laboratory Research and Development Report*, No. DTMB-1143, David Taylor Model Basin, Washington DC.

Han, K., Y.T. Feng, and D.R.J. Owen, 2010, Three-dimensional modelling and simulation of magnetorheological fluids, *Int. J. Numer. Methods Eng.* **84**, 1273-1302.

Hato, M.J., H.J. Choi, H.H. Sim, B.O. Park, and S.S. Ray, 2011, Magnetic carbonyl iron suspension with organoclay additive and its magnetorheological properties, *Colloids Surf., A-Physicochem. Eng. Asp.* **377**, 103-109.

Jang, I.B., H.B. Kim, J.Y. Lee, J.L. You, H.J. Choi, and M.S. Jhon, 2005, Role of organic coating on carbonyl iron suspended particles in magnetorheological fluids, *J. Appl. Phys.* **97**, 10Q912.

Jolly, M.R., J.W. Bender, and J.D. Carlson, 1999, Properties and applications of commercial magnetorheological fluids, *J. Intell. Mater. Syst. Struct.* **10**, 5-13.

Kozlowska, J. and M. Leonowicz, 2013, Magnetorheological fluids as a prospective component of composite armours, *Compos. Theory and Pract.* **13**, 227-231.

Kruggel-Emden, H., E. Simsek, S. Rickelt, S. Wirtz, and V. Scherer, 2007, Review and extension of normal force models for the discrete element method, *Powder Technol.* **171**, 157-173.

Kruggel-Emden, H., S. Wirtz, and V. Scherer, 2008, A study on tangential force laws applicable to the discrete element method (DEM) for materials with viscoelastic or plastic behavior, *Chem. Eng. Sci.* **63**, 1523-1541.

Lim, S.T., H.J. Choi, and M.S. Jhon, 2005, Magnetorheological characterization of carbonyl iron-organoclay suspensions, *IEEE Trans. Magn.* **41**, 3745-3747.

López-López, M.T., G. Vertelov, G. Bossis, P. Kuzhir, and J.D.G. Durán, 2007, New magnetorheological fluids based on magnetic fibers, *J. Mater. Chem.* **17**, 3839-3844.

Loth, E., 2008, Drag of non-spherical solid particles of regular and irregular shape. *Powder Technol.* **182**, 342-353.

Ly, H.V., F. Reitich, M.R. Jolly, H.T. Banks, and K. Ito, 1999, Simulations of particle dynamics in magnetorheological fluids, *J. Comput. Phys.* **155**, 160-177.

Maxey, M.R., B.K. Patel, E.J. Chang, L.P. Wang, 1997, Simulations of dispersed turbulent multiphase flow, *Fluid Dyn. Res.* **20**, 143-156.

McManus, S.J., K.S. Clair, P.E. Boileau, J. Boutin, and S. Rakheja, 2002, Evaluation of vibration and shock attenuation performance of a suspension seat with a semi-active magnetorheological fluid damper, *J. Sound Vibr.* **253**, 313-327.

Phule, P.P., 2001, Magnetorheological (MR) fluids: Principles and applications, *Smart Mater. Bull.* **2001**, 7-10.

Pöschel, T. and T. Schwager, 2005, *Computational Granular Dynamics: Models and Algorithms*, Springer-Verlag Berlin Heidelberg, New York.

Ren, B., W. Zhong, Y. Chen, X. Chen, B. Jin, Z. Yuan, and Y. Lu, 2012, CFD-DEM simulation of spouting of corn-shaped particles, *Particuology* **10**, 562-572.

Shah, K. and S.-B. Choi, 2015, The influence of particle size on the rheological properties of plate-like iron particle based magnetorheological fluids, *Smart Mater. Struct.* **24**, 015004.

Son, K.J. and E.P. Fahrenthold, 2012, Evaluation of magnetorheological fluid augmented fabric as a fragment barrier material, *Smart Mater. Struct.* **21**, 075012.

Son, K.J. and E.P. Fahrenthold, 2014, Simulation of orbital debris impact on porous ceramic tiles, *J. Spacecr. Rockets* **51**, 1349-1359.

Sun, R. and H. Xiao, 2016, SediFoam: A general-purpose, open-source CFD-DEM solver for particle-laden flow with emphasis on sediment transport, *Comput. Geosci.* **89**, 207-219.

Tsuji, Y., T. Tanaka, and T. Ishida, 1992, Lagrangian numerical simulation of plug flow of cohesionless particles in a horizontal pipe, *Powder Technol.* **71**, 239-250.

Wu, W.P., B.Y. Zhao, Q. Wu, L.S. Chen, and K.A. Hu, 2006, The strengthening effect of guar gum on the yield stress of magnetorheological fluid, *Smart Mater. Struct.* **15**, N94-N98.

Yao, G.Z., F.F. Yap, G. Chen, W.H. Li, and S.H. Yeo, 2002, MR damper and its application for semi-active control of vehicle suspension system, *Mechatronics* **12**, 963-973.

Zhang, W.L., Y.D. Liu, and H.J. Choi, 2012, Field-responsive smart composite particle suspension: Materials and rheology, *Korea-Aust. Rheol. J.* **24**, 147-153.